Quasi-Decadal Variability of the Stratosphere: Influence of Long-Term Solar Ultraviolet Variations

L. L. HOOD

Lunar and Planetary Laboratory, University of Arizona, Tucson, Arizona

J. L. JIRIKOWIC

Department of Geosciences, University of Arizona, Tucson, Arizona

J. P. MCCORMACK

Department of Atmospheric Sciences, University of Arizona, Tucson, Arizona

(Manuscript received 24 November 1992, in final form 10 March 1993)

ABSTRACT

A multiple regression statistical model is applied to investigate the existence of upper-stratospheric ozone, temperature, and zonal wind responses to long-term (solar cycle) changes in solar ultraviolet radiation using 11.5 years of reprocessed *Nimbus-7* Solar Backscattered Ultraviolet (SBUV) data and 12.4 years of National Meteorological Center (NMC) data. A positive solar cycle variation of independently measured ozone and temperature occurs with maximum amplitude near the low-latitude stratopause. The seasonal solar regression coefficients near 1 mb for both ozone and temperature occur at low latitudes supporting a role for photochemical and radiative forcing in their origin. Zonal wind perturbations that correlate with long-term solar ultraviolet variations are a strong function of season and pressure level. Above ~2 mbar, the largest solar-correlated zonal wind enhancements occur at middle winter latitudes near the time of winter solstice in both hemispheres. The Northern Hemisphere December enhancement at 1 mb was especially large, 23 ± 9 m s^{-1} from solar minimum to maximum during the last solar cycle. The derived ozone, temperature, and zonal wind increases with increasing solar ultraviolet flux near the stratopause are larger than predicted by models that consider primarily photochemical and radiative processes. The higher ozone and temperature response amplitudes at low latitudes may be due to modified ozone transport and adiabatic temperature changes induced by the dynamical response. If the midlatitude winter solstice wind enhancements are solar induced, their high amplitudes require a positive feedback due to wave–mean flow interaction such that the planetary wave drag on the flow is reduced under solar maximum conditions.

1. Introduction

It is well known theoretically that changes in solar ultraviolet spectral irradiance can perturb the chemical, thermal, and dynamical structure of the upper stratosphere and mesosphere (e.g., Brasseur and Solomon 1984; Callis et al. 1985). Solar ultraviolet variations occur primarily on the ~27-day time scale (due to the development of active regions on the solar disk modulated by solar rotation) and on the time scale of the 10–11-year solar activity cycle (Donnelly et al. 1983; Donnelly 1991; Cebula et al. 1992). On the active region time scale, available satellite datasets span many solar rotations so that middle atmospheric ozone and temperature responses to short-term solar UV variations are relatively well documented (Gille et al. 1984; Hood 1984, 1986; Keating et al. 1985; Keating et al. 1987; Chandra 1986; Hood and Jirikowic 1991; Hood et al. 1991). However, on the more important solar cycle time scale, measurement records for the middle and lower stratosphere span no more than three or four cycles and high quality global measurements for the upper stratosphere (where the most direct UV effects are expected) span only slightly more than one cycle. Nevertheless, recent studies of column ozone measurements obtained with the *Nimbus-7* Total Ozone Mapping Spectrometer (TOMS) over a 13-year interval have identified an apparent solar cycle variation of stratospheric total ozone (Chandra 1991; Stolarski et al. 1991; Hood and McCormack 1992).

An initial observation suggesting that the upper-stratospheric response to solar cycle changes in ultraviolet radiation may be somewhat larger than expected theoretically was reported by Kodera and Yamazaki (1990). Using a combination of rocket measurements and National Meteorological Center (NMC) derived

Corresponding author address: Lon L. Hood, Department of Planetary Sciences, Lunar and Planetary Laboratory, University of Arizona, Tucson, AZ 85721.

zonal winds, these authors found an apparent relatively large (>20 m s^{-1}) variation of the December zonal wind near the stratopause at 40°N in phase with the solar activity cycle during an observation period covering approximately two cycles. Since the latitudinal gradient of radiative heating reaches a maximum near the stratopause at middle latitudes under winter solstice conditions, this correlation was in qualitative agreement with the hypothesis of solar ultraviolet forcing. However, the amplitude of the variation was much larger than predicted from models that consider radiative heating changes alone. For example, Kodera et al. (1990) and Kodera et al. (1991a) showed that a >30% solar cycle change in radiative heating due to ozone absorption of solar UV radiation would be required to reproduce the observed December wind variation in a general circulation model. Such a heating variation is implausible given current empirical limits on the solar cycle change in ultraviolet spectral irradiance (Donnelly 1991; Cebula et al. 1992).

Given that a December stratopause wind variation of the observed amplitude occurs (whether or not solar ultraviolet forcing is responsible), Kodera et al. (1990) have used both observations and GCM simulations to show that derivative effects on lower-stratospheric and upper-tropospheric circulation follow later in the winter at middle and high latitudes. Kodera (1991) and Kodera et al. (1991a) also carried out numerical experiments to show that a combination of the observed December wind variation and a prescribed equatorial quasi-biennial wind oscillation (QBO) could result in temperature anomalies that are similar in many respects to those reported by Labitzke and van Loon (1988). The latter authors have described a tendency for midwinter middle-stratospheric temperatures at high latitudes to vary approximately in phase with the solar cycle (during the 3.5-cycle observation period) when the data were sorted according to the phase of the equatorial QBO at 50 mbar (see also Labitzke 1982; van Loon and Labitzke 1990). Most of the correlation was related to the occurrence or absence of major midwinter warmings during individual years. This reported correlation has been challenged on statistical grounds (Salby and Shea 1991; Baldwin and Dunkerton 1989). However, it has also been found that empirical models of stratospheric interannual variability are most successful when they include both the QBO and a "quasi-decadal variation" that is in phase with the solar cycle. (Dunkerton and Baldwin 1992).

If solar ultraviolet variations are capable of inducing significant changes in midlatitude December zonal wind near the stratopause, then changes in the chemical and thermal structure of the upper stratosphere should also be observable. To test this hypothesis and obtain more quantitative constraints on model simulations of the December wind variation, it is necessary to analyze upper-stratospheric ozone and temperature data as well as derived zonal winds. The selected datasets should extend over at least one solar activity cycle and should ideally have global coverage over an altitude range reaching at least to the stratopause. Two independent satellite records that appear to meet these criteria are the U.S. NMC temperature dataset (Gelman et al. 1986) and the *Nimbus-7* Solar Backscattered Ultraviolet (SBUV) ozone profile dataset (e.g., McPeters and Komhyr 1991). The NMC data have incorporated global satellite measurements extending up to 1 mbar since 24 September 1978; a reprocessed version of this dataset including derived circulation statistics has been compiled by Randel (1992) for a continuous period through February 1991 (12.4 years). A reprocessed version of the *Nimbus-7* SBUV ozone dataset extends from January 1979 to June 1990 (11.5 years) (R. D. McPeters 1992, personal communication).

In section 2, the SBUV ozone and NMC temperature datasets and the processing procedures applied to these datasets are described. In section 3, the calculated long-term mean seasonal variations of ozone, temperature, and zonal wind in the upper stratosphere are briefly discussed for later reference. A multiple regression statistical model is employed in section 4 to separate approximately the QBO, solar cycle, and long-term trend components of interannual stratospheric ozone, temperature, and zonal wind change using the SBUV and NMC data. The solar component results of the statistical analysis are then presented as a function of latitude and season. Some interpretations and comparisons with model calculations are given in section 5, followed by conclusions in section 6.

2. Data description

a. SBUV and NMC datasets

The *Nimbus-7* SBUV instrument is a nadir-viewing double monochromator that samples backscattered irradiances at 12 wavelengths in the Hartley and Huggins absorption bands from which the ozone profile may be inferred (Heath et al. 1975). Vertical resolution is fixed principally by the effective width of the scattering layer and is approximately 8 km (McPeters et al. 1984). The uppermost level for which useful ozone measurements were obtained is limited by the shortest sampled wavelength used for profile inversion and has been calculated to be in the range of 0.8–1.1 mb for solar zenith angles of 40° to 60° (Frederick et al. 1983). The lowest useful measurement altitude is well below the lowest level considered here (~10 mb). Although instrument-related drifts have complicated the interpretation of long-term trends in the SBUV data, recent improvements in adjustment procedures by the NASA Ozone Processing Team have resulted in an SBUV dataset with better long-term stability (Herman et al. 1991; McPeters and Komhyr 1991). The Version 6 SBUV dataset analyzed here consists of monthly zonal means for an 11.5-year period, January 1979 to June 1990 (R. D. McPeters 1992, personal communication).

Possible remaining artificial linear trends in the SBUV data are of no significant concern since the record length exceeds one solar cycle and linear trends are removed by regression as part of the analysis. Figure 1a shows an area-weighted average of SBUV ozone measurements for a layer between 0.5 and 1 mbar and for latitudes between 65°S and 65°N. A nearly linear negative trend is present in the original data but has been removed by regression before plotting in Fig. 1a. The ozone measurements are given in terms of the total ozone column amount within the 0.5–1-mb layer in Dobson units (DU). Because the ozone concentration increases rapidly with decreasing altitude near the stratopause, the ozone amount for this layer is very nearly proportional to the ozone concentration near 1 mbar. Similar measurements within layers of 1–2 mb, 2–4 mb, and 4–8 mb will be employed later in this paper to investigate interannual ozone changes at different levels in the upper stratosphere.

Prior to 1978, continuous stratospheric temperature measurements with large-scale geographic coverage were mainly limited to levels below 10 mbar where routine balloon soundings are possible. However, beginning on 24 September 1978, global satellite records extending up to 1 mb began to be included in the National Oceanic and Atmospheric Administration (NOAA) NMC daily analyses. Prior to 17 October 1980, the archived temperatures were based on simple regressions relating temperature at stratospheric levels to measurements from two channels of either the *NOAA-5* Vertical Temperature Profiler Radiometer (9/24/78–2/23/79), the *TIROS N* Stratospheric Sounding Unit (SSU) (2/25/79–1/20/80), or the *NOAA-6* SSU (1/21/80–10/16/80) (Gelman et al. 1983). Beginning on 17 October 1980, an improved modified Cressman analysis system was begun employing measurements from nine channels on three different instruments, including the SSU, that make up the TIROS Operational Vertical Sounder (TOVS) unit. This system continues to be operational to the present using data from a series of operational polar orbiters carrying TOVS units (Gelman et al. 1986; Finger et al. 1993). The vertical resolution of the derived temperature retrievals in the upper stratosphere is limited mainly by the effective widths of the scattering layers or contribution functions for SSU channels 2 and 3 (Smith et al. 1979) and is comparable to that of the SBUV retrievals (i.e., 5 to 10 km).

The actual version of the NMC data analyzed here has been described by Randel (1992) and consists of daily (1200 UTC) geopotential height grids from 10 to 1 mbar (approximately 32 to 48 km altitude) for a time interval from October 1978 to February 1991. The height grids are produced by the NMC Climate Analysis Center (CAC) and are stored in the form of zonal Fourier coefficients, assigned to a 40-point Gaussian grid in latitude with mean spacing of approximately 4.5°. For the calculation of temperatures and zonal winds from the archived geopotential height grids, the methods of Randel (1992) are adopted. Temperature is calculated from the hydrostatic relation (involving vertical derivatives of geopotential height) and zonal mean zonal wind is calculated from gradient balance, representing an improvement over geostrophic balance (e.g., Randel 1987). Linear interpolation is used to assign winds within 7° of the equator. Some error (e.g., smoothing) in derived equatorial winds may result from this procedure.

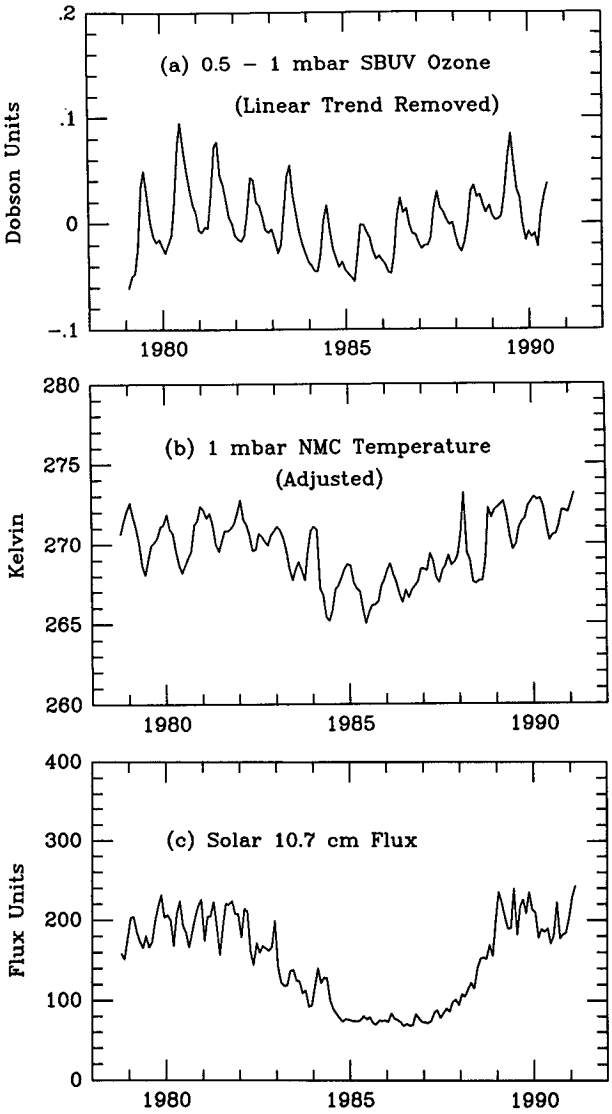

FIG. 1. (a) Time series of area-weighted averages of monthly zonal mean *Nimbus-7* SBUV ozone column density within the layer 0.5–1 mb and at latitudes between 65°S and 65°N after subtracting the linear trend. (b) Time series of area-weighted averages of monthly zonal mean NOAA NMC temperature at the 1-mb level for latitudes between 65°S and 65°N after adjustment to rocket measurements as described in the text. (c) Monthly mean solar 10.7-cm flux, a ground-based proxy for long-term solar ultraviolet variations.

b. *Adjustments to the temperature data*

At the 10-mb level, balloonsonde data allow continuous updating of satellite retrieval regression coefficients at intervals of 1 to 4 weeks. This procedure minimizes errors due to the several modifications of the NMC operational analysis scheme and changes of operational satellites that occurred during the 12.4-year analysis period. However, at levels above 10 mbar (5, 2, and 1 mbar), the data are derived entirely from satellite temperature retrievals and the regression coefficients are held constant. In order to minimize effects of operational satellite changes, etc., at these higher levels, the procedures of Gelman et al. (1986) and Finger et al. (1993) are adopted to adjust the archived NMC temperatures based on comparisons of satellite radiance temperatures with collocated rocketsonde temperatures. The required adjustment coefficients (from Finger et al. 1993) are listed in Table 1. As described by Gelman et al., prior to 17 October 1980, a temperature adjustment that is linear in latitude was employed in order to match all of the available rocketsonde data in the Northern Hemisphere. Although most rocketsonde stations were located at northern middle latitudes, the same adjustment was extrapolated to southern latitudes as well. After 17 October 1980, when the improved TOVS system was introduced, an adjustment that was independent of latitude was found to be adequate.

After application of the adjustment coefficients listed in Table 1 to the NMC zonal mean temperature data, approximately constant offsets were visually evident at many latitudes and pressure levels for the data prior to 17 October 1980 as compared to the data after this date. We interpret this to be an artificial consequence of the relative absence of rocketsonde measurements in the tropics and Southern Hemisphere and of the changeover to a constant coefficient system when the TOVS system was begun. We therefore minimized these offsets by regression fits on either side of the 17 October 1980 date [see Gelman et al. (1986) for further discussion of offset removal techniques]. Also, at the 1-mb level, a large temperature spike was present at most latitudes centered on January 1984 that appears to be artificial, based on comparisons with other years and with SBUV ozone measurements (which tend to be inversely correlated with temperature on time scales <1 year in the upper stratosphere). This spike was therefore removed by linear interpolation at each affected latitude. No other adjustments were applied. Figure 1b shows an area-weighted average of the resulting 1-mb NMC temperature measurements between 65°S and 65°N. This latitude range was chosen to be consistent with that used for the SBUV ozone average of Fig. 1a.

TABLE 1. NMC temperature adjustment coefficients and standard errors. From Gelman et al. (1986) and Finger et al. (1993). Prior to 10/17/80, adjusted temperature is defined by $T_{adj} = T_{NMC} - A - BL$, where L is absolute latitude in degrees (positive in both hemispheres), A is in kelvin, and B is in kelvin per degree. After 10/17/80, adjusted temperature is defined by $T_{adj} = T_{NMC} - C$, where C is in kelvin.

Start date	End date	A	B	C
		(a) 1 mb		
9/24/78	2/22/79	−0.16 ± 0.93	−0.02 ± 0.02	—
2/25/79	1/20/80	−1.8 ± 0.40	−0.06 ± 0.01	—
1/21/80	10/16/80	−0.92 ± 0.44	−0.04 ± 0.01	—
10/17/80	9/1/81	—	—	−7.0 ± 0.5
9/2/81	9/1/83	—	—	−8.3 ± 0.4
9/2/83	6/18/84	—	—	−5.4 ± 0.4
6/19/84	2/26/85	—	—	−4.0 ± 1.4
3/27/85	3/10/87	—	—	−7.3 ± 0.5
3/11/87	9/19/88	—	—	−6.6 ± 0.5
9/20/88	—	—	—	−6.2 ± 0.5
		(b) 2 mb		
9/24/78	2/22/79	0.30 ± 0.59	−0.06 ± 0.02	—
2/25/79	1/20/80	−4.71 ± 0.29	0.02 ± 0.01	—
1/21/80	10/16/80	−6.04 ± 0.40	0.06 ± 0.01	—
10/17/80	9/1/81	—	—	−3.2 ± 0.5
9/2/81	9/1/83	—	—	−1.1 ± 0.3
9/2/83	6/18/84	—	—	−4.9 ± 0.5
6/19/84	2/26/85	—	—	−3.7 ± 1.2
3/27/85	3/10/87	—	—	−3.3 ± 0.4
3/11/87	9/19/88	—	—	−3.3 ± 0.4
9/20/88	—	—	—	−2.4 ± 0.3
		(c) 5 mb		
9/24/78	2/22/79	−0.19 ± 0.68	−0.03 ± 0.02	—
2/25/79	1/20/80	−4.05 ± 0.28	0.07 ± 0.01	—
1/21/80	10/16/80	−5.14 ± 0.31	0.08 ± 0.01	—
10/17/80	9/1/81	—	—	2.2 ± 0.4
9/2/81	9/1/83	—	—	5.7 ± 0.6
9/2/83	6/18/84	—	—	−0.5 ± 0.6
6/19/84	2/26/85	—	—	1.9 ± 1.3
3/27/85	3/10/87	—	—	5.7 ± 0.4
3/11/87	9/19/88	—	—	4.6 ± 0.3
9/20/88	—	—	—	2.2 ± 0.3

c. *Interannual solar ultraviolet variations*

Measurements of the solar cycle change in ultraviolet spectral irradiance are more difficult than those on the solar rotation time scale because of the existence of long-term, wavelength-dependent drifts due to degradation with time of spacecraft instruments in the harsh space environment [for a review, see Lean (1991)]. However, a means has been devised to closely estimate the solar cycle UV irradiance change by using satellite measurements of the ratio of the solar irradiance at the core of the Mg II h and k absorption lines near 280 nm to that at a nearby wavelength in the unabsorbed continuum, the Mg II core-to-wing ratio (Heath and Schlesinger 1986). The emission in the line core originates at high levels in the solar photosphere near where the continuum emission at shorter wavelengths (e.g., near 200 nm) originates. The emission in the line wings originates at lower levels in the photosphere where there is nearly no temporal variability. Ratioing these two

irradiances at closely spaced wavelengths nearly eliminates any long-term drift in the data. Because the line core emission has nearly the same temporal variability as the continuum emission at wavelengths near 200 nm, the Mg II core-to-wing ratio provides the best available measure of solar cycle changes in ultraviolet radiation at photochemically important wavelengths. Current estimates for the solar ultraviolet irradiance change near 205 nm between solar minimum in 1986 and solar maximum in 1990 based on the Mg II index range from about 7% (Donnelly 1991) to about 10% (Cebula et al. 1992). The difference stems from slightly different definitions of the index and different approaches to the analysis of *Nimbus-7* and *NOAA-9* solar ultraviolet data. The solar cycle irradiance variation falls off rapidly with increasing wavelength but the variations at different wavelengths are observed (at least on the solar rotation time scale) to be highly uniform with amplitudes that differ from one another by a nearly constant factor at each wavelength (Donnelly 1988). For instance, a 1% change in flux at 205 nm is accompanied by a change of ~0.4% at 250 nm, etc.

For the purposes of this paper, it is sufficient to consider a well-known ground-based proxy for solar ultraviolet variations, the solar radio flux at 10.7 cm (F10.7), available from the National Geophysical Data Center, Boulder, Colorado. On time scales >1 month, F10.7 has been found to be closely correlated with solar ultraviolet radiation variations at stratospherically important wavelengths (Donnelly 1991). As shown in Fig. 1c, F10.7 varied by more than 130 flux units between solar minimum and maximum during the last solar cycle. Thus, a 130 unit change of F10.7 is equivalent to a 7% to 10% change in solar UV flux at 205 nm. Comparing Figs. 1a, 1b, and 1c, it is seen that the globally averaged ozone and temperature data near 1 mb vary approximately in phase with F10.7 during the last solar cycle.

3. Upper-stratospheric seasonal variations

To provide a context for the interpretation of multiple regression statistical analyses presented in the next section, Fig. 2 shows the dependence on latitude and season of the long-term mean for zonally averaged ozone, temperature, and derived zonal wind at 1 mbar. As shown in Fig. 2a, the ozone column amount within the 0.5–1-mb layer maximizes at high latitudes in the winter hemisphere and reaches a minimum at high latitudes in the summer hemisphere. A comparison of the ozone seasonal variation with that of temperature in Fig. 2b suggests that the ozone seasonal variation is at least partly a response to the seasonal temperature variation. This is plausible since ozone is near photochemical equilibrium at this level and the ozone concentration tends to vary inversely with temperature due to the exponential temperature dependences of dominant reaction rates (e.g., Brasseur and Solomon 1984).

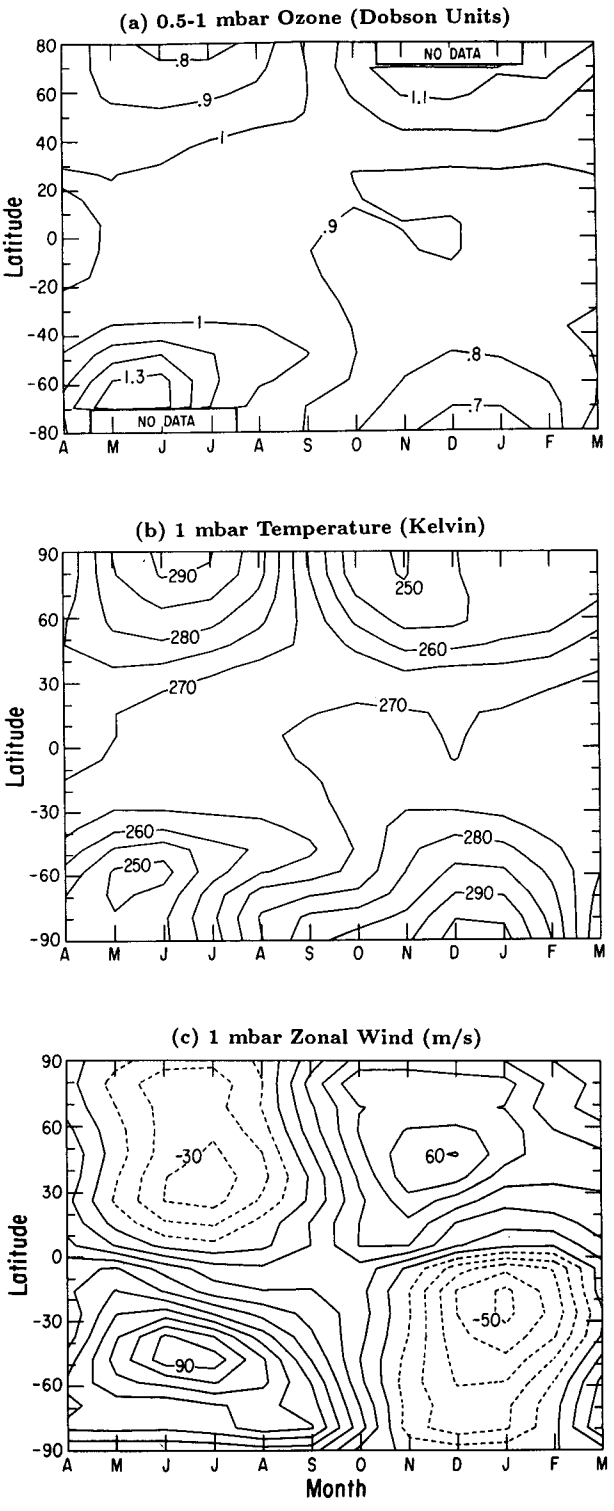

FIG. 2. (a) Long-term (11.5-year) mean of monthly zonal mean *Nimbus-7* SBUV ozone within the layer 0.5–1 mb plotted as a function of latitude and month (April, May, etc.). (b) Long-term (12.4 yr) mean of monthly zonal mean NMC temperature at 1 mb. (c) Long-term (12.4 yr) mean of monthly zonal mean zonal wind at 1 mb derived from the NMC data using the gradient wind algorithm of Randel (1992).

Some contribution of eddy transport to the high-latitude winter ozone increases is also likely, however.

The seasonal variation of zonal mean temperature (Fig. 2b) at 1 mbar is characterized by minima at high latitudes in winter and maxima at high latitudes in summer. As discussed, for example, by Andrews et al. (1987), the summer temperature maxima are nearly the same as that predicted by radiative equilibrium calculations (e.g., Fels 1985) and are therefore explicable in terms of the seasonal variation of radiative heating and cooling. However, the 1-mb winter temperature minima at high latitudes are larger by nearly 100° than the predictions of radiative equilibrium calculations and require a substantial dynamical heating component. The dynamical heating component of the seasonal variation is believed to occur primarily due to interaction of the mean flow with transient planetary-scale Rossby waves in the winter stratosphere. These waves are orographically forced and are therefore stationary relative to the earth so that wave absorption results in a deceleration of the flow. The consequent negative zonal wind acceleration and associated meridional motions lead to increased downwelling and adiabatic heating near the winter pole. Breaking gravity waves, which dominantly determine the circulation and thermal structure of the winter mesosphere, are believed to be less important in the winter upper stratosphere than are planetary-scale Rossby waves but they could still play a secondary role.

The seasonal variation of zonal mean zonal wind at 1 mb computed from Randel's (1992) gradient wind algorithm under the assumption of thermal wind balance is shown in Fig. 2c. Positive (westerly) zonal wind maxima occur at middle latitudes near the winter solstices (December in the NH and June/July in the SH). The northern mean winter wind maximum of ~60 m s^{-1} is less than the corresponding southern maximum of ~95 m s^{-1} because of the increased amplitudes of orographically forced, stationary planetary waves in the NH, which tend to decelerate the wind through wave transience and dissipation. Similarly, negative wind maxima occur under summer solstice conditions with smaller mean easterly winds of ~ −35 m s^{-1} in the NH as compared to the SH (~ −50 m s^{-1}). The greater amplitude of the winter westerlies relative to the summer easterlies is a consequence of the stronger latitudinal gradient of radiative heating near the winter solstice, as exemplified by the contrast between the polar night and the sunlit atmosphere.

4. Multiple regression analysis

a. Statistical model

On interannual time scales, stratospheric ozone concentration, temperature, and zonal wind can vary in response to a number of competing factors, including 1) changes in the internal dynamics of the atmosphere–ocean system [e.g., the QBO and the El Niño/Southern Oscillation (ENSO)]; 2) changes in solar ultraviolet radiation and other external effects such as energetic particle precipitation; 3) anthropogenic trends in the concentration of important trace gases including chlorofluorocarbons (CFC) and CO_2; and 4) changes in the abundance of volcanically ejected trace gases and aerosols (e.g., World Meteorological Organization 1988). At different levels in the upper stratosphere, each of the above forcing mechanisms can be significant. For example, a quasi-biennial modulation of interannual temperature, zonal wind, and associated ozone variations is detectable for many latitude bands (e.g., Baldwin and Dunkerton 1991). At lower levels in the upper stratosphere, positive temperature and ozone anomalies occur at some latitudes during 1982 and 1983 in association with the El Chichón volcanic eruption (e.g., Pollack and Ackerman 1983). Although not studied in detail here, a temperature (or radiance) anomaly associated with El Chichón (and/or with the 1982–83 ENSO event) is prominent in the NMC temperature data and, to a lesser extent, in the SBUV ozone data at lower levels in the upper stratosphere. Previous studies of rocket temperature soundings spanning several decades have obtained evidence for long-term cooling trends in the upper stratosphere that may be attributed to anthropogenic CO_2 increases (Angell 1991). Cooling trends are present in the NMC temperature data at several levels in the upper stratosphere. Finally, theoretical expectations and data such as that shown in Fig. 1 indicate that solar ultraviolet variations may produce changes in stratospheric temperature and ozone, especially at the highest levels in the upper stratosphere. Detailed study of the latter effects therefore requires simultaneous estimates for effects of each of the other major sources of stratospheric interannual variability.

In order to examine in more detail the possible response of the upper stratosphere to interannual changes in solar ultraviolet flux, we consider a linear statistical model for the temporal behavior of zonally averaged ozone, temperature, and zonal wind. Trial calculations indicate that a relatively simple model consisting of only linear trend, solar cycle, and QBO components is sufficient for an initial investigation. Specifically, we consider a model of the form

$$Y(t) = \mu(i) + \beta_T t + \beta_{\mathrm{QBO}} X_{\mathrm{QBO}}(t - L) + \beta_{\mathrm{SUN}} X_{\mathrm{SUN}}(t) + \epsilon(t), \quad (1)$$

where t is the time in months, $Y(t)$ represents zonal mean ozone, temperature, or zonal wind at a given pressure level and latitude, $\mu(i)$ is a seasonal term equal to the long-term mean for the ith month of the year ($i = 1, 2, \cdots, 12$), $X_{\mathrm{QBO}}(t)$ is a time series representing the tropical quasi-biennial oscillation (QBO), L is the optimum phase lag between $X_{\mathrm{QBO}}(t)$ and $Y(t)$, X_{SUN} is a time series representing solar variability (no phase lag is assumed), $\epsilon(t)$ is a residual error term, and β_T,

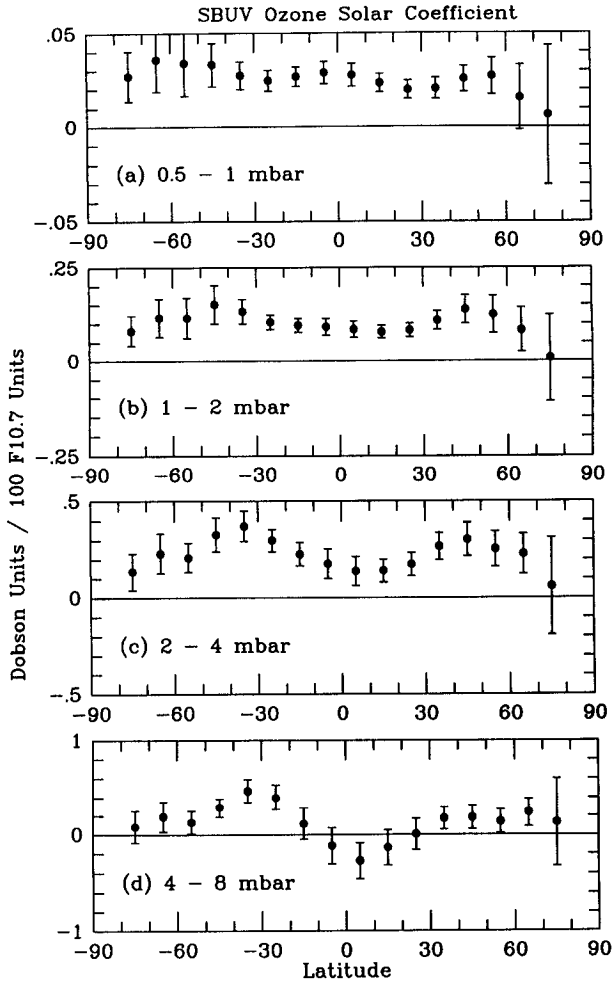

FIG. 3. Solar regression coefficient β_{SUN} calculated from 138 months of zonal mean SBUV ozone data for the indicated pressure layers by generalized least squares using the statistical model represented by Eq. (1). The error bars are two standard deviations.

β_{QBO}, and β_{SUN} are coefficients to be determined by least-squares regression. To represent the QBO, the Singapore (2°N) 30-mb zonal wind (J. Angell 1992, personal communication) is used. To represent solar variability, the F10.7 time series of Fig. 1c is adopted. Applications of (1) to these stratospheric time series without specifying the error term $\epsilon(t)$ generally yield residuals that are first-order autocorrelated. We have therefore modeled the error term as a first-order autoregressive process, that is, $\epsilon(t) = r\epsilon(t-1) + w(t)$, where $w(t)$ is white noise; r is estimated from an initial application of (1), and remaining coefficients are determined in a second application by generalized least squares (e.g., Neter et al. 1985).

b. *Regression results versus latitude*

Initially, we consider the entire record of NMC temperature (149 months) and SBUV ozone (138 months) without separating the data according to season. Analysis of derived zonal winds is deferred to the next subsection. Figures 3 and 4 are the resulting annual mean ozone and temperature solar regression coefficients plotted versus latitude at each available pressure level (or layer in the case of ozone). The error bars are two standard deviations in length.

As shown in Fig. 3, the ozone regression coefficients are positive and nearly constant with latitude at 1 mbar but are a stronger function of latitude at lower altitudes in the upper stratosphere. At low latitudes, the regression coefficient decreases with decreasing altitude and becomes slightly negative near the equator in the 4–8-mb layer. At middle latitudes, the regression coefficient remains significantly positive in all layers but begins to diminish in amplitude in the 4–8-mb layer. As shown in Fig. 4, the temperature regression coefficient at latitudes $< 35°$ is strong and positive at 1 mbar but decreases rapidly with decreasing altitude in the upper

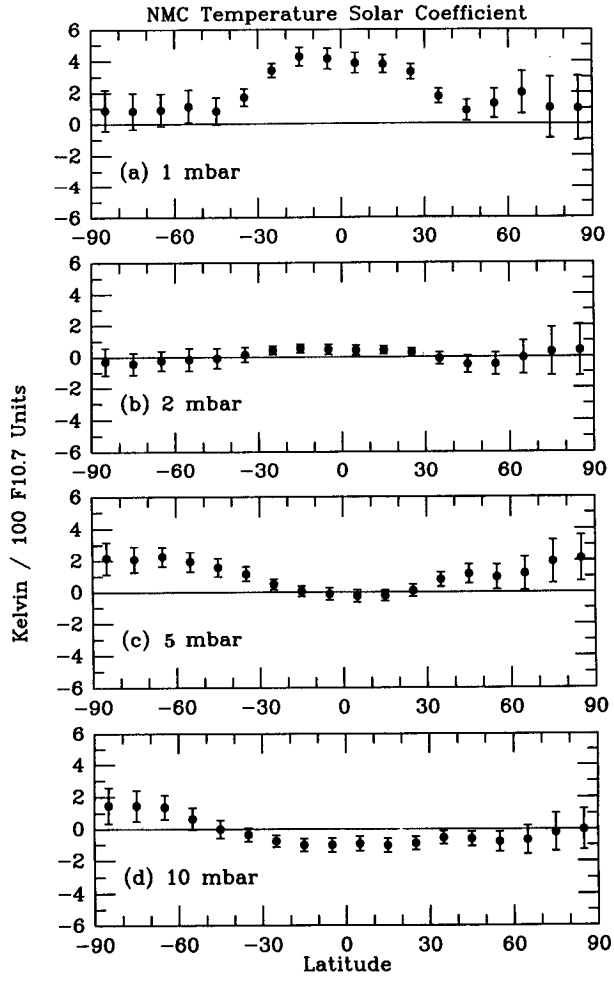

FIG. 4. Solar regression coefficient calculated from 149 months of adjusted NMC zonal mean temperature data for the indicated pressure layers using Eq. (1). The error bars are two standard deviations.

stratosphere, becoming slightly negative by 10 mbar. At latitudes > 35°, the regression coefficients are not significantly different from zero at 1 and 2 mb but become significantly positive at 5 and 10 mb.

c. *Regression results versus season*

The dependence of the SBUV ozone, NMC temperature, and derived zonal wind solar regression coefficients on season was investigated by applying the statistical model (1) to zonal means at individual latitude bands and pressure levels for each of the 12 months. For this application, the seasonal term $\mu(i)$ in (1) is unnecessary. Only 11 to 13 data points are available for analysis (depending on the month and the dataset) leading to larger 2σ error estimates than for the annual mean results of Figs. 3 and 4. Nevertheless, statistically significant (at the 2σ level) regression coefficients are found for at least some months and latitudes at each pressure level. These statistically significant coefficients are not randomly distributed but are physically related in most cases as discussed in the next section.

Figure 5 displays the solar regression coefficients at the 1-mb level calculated as described above as a function of latitude and season. Shaded areas are not significantly different from zero at the 2σ level. The ozone coefficient contour map in the top panel contains a curved band of significantly positive values mainly at low latitudes. For comparison, the line of zero solar zenith angle is indicated by the long-dashed curve. Several large positive coefficient maxima occur at high latitudes in December and June that are significant at the 2σ level. As shown in the center panel, there is also a band of positive temperature regression coefficients at low latitudes. This band exhibits a slight tendency to follow the line of zero solar zenith angle. However, a quantitative analysis (section 5) indicates that the observed temperature variation is too large to be due to radiative forcing alone. Most of the temperature coefficients at high latitudes are not significant at this pressure level in agreement with the annually averaged coefficients in the top panel of Fig. 4. As shown in the lower panel of Fig. 5, the largest positive zonal wind solar coefficient ($\sim$18 m s^{-1} per 100 units of F10.7) occurs at middle northern latitudes in December. This result is in qualitative agreement with the December wind anomaly reported by Kodera and Yamazaki (1990) discussed in the Introduction. In addition, a second relatively strong coefficient maximum ($\sim$14 m s^{-1} per 100 units of F10.7) occurs at middle southern latitudes in June and July. Other weaker negative (easterly) wind coefficient maxima are also present that are significant at the 2σ level.

To provide a better appreciation for the interannual variability within which the apparent solar-related winter solstice wind variations are embedded, Fig. 6 shows the observed winds in time series form. The 1-mb statistical model estimates including the first-order

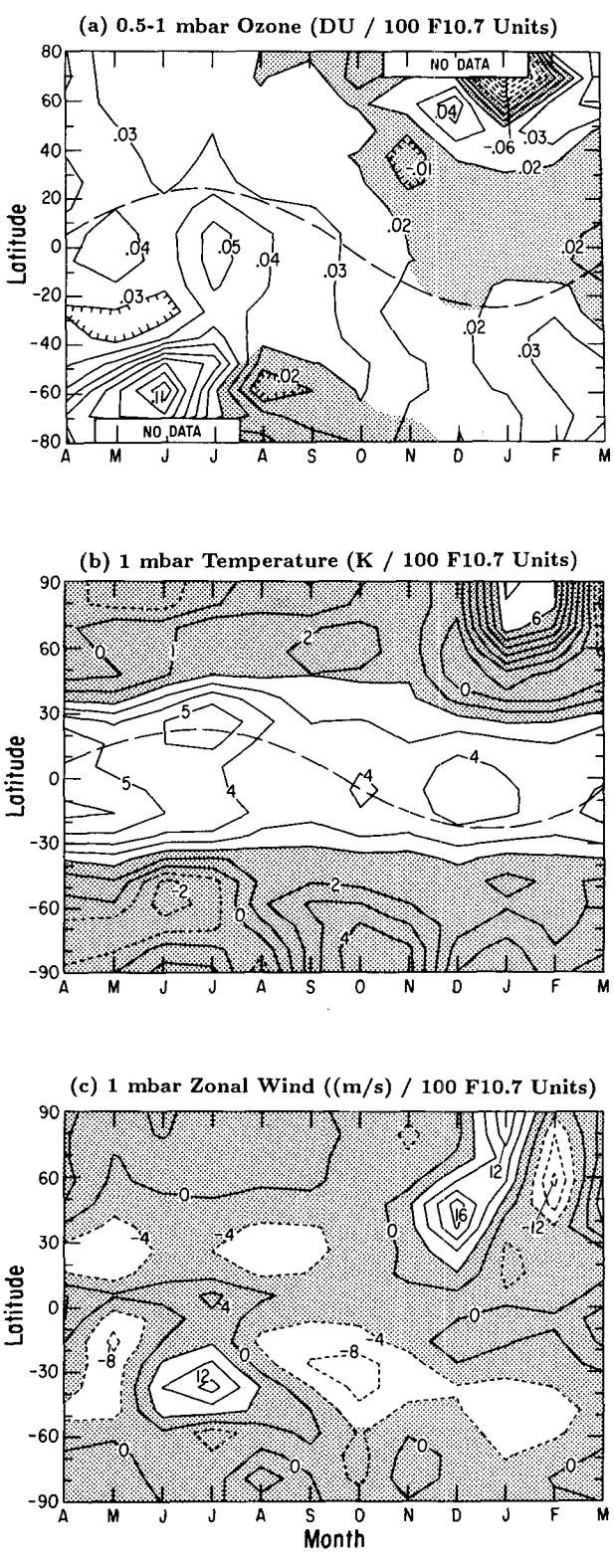

FIG. 5. Monthly solar regression coefficients for (a) SBUV ozone at 0.5–1 mb, (b) NMC temperature at 1 mb, and (c) derived zonal wind at 1 mb. Values within shaded areas are not statistically significant at the 2σ level. The long-dashed line in the top two panels is the line of zero solar zenith angle.

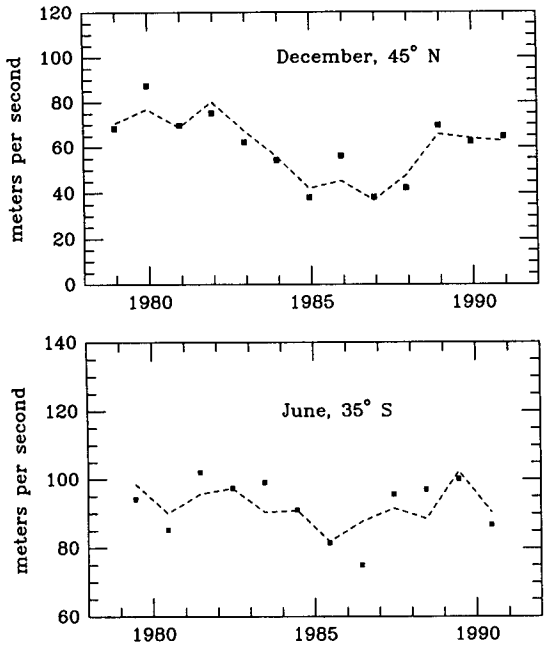

FIG. 6. The solid squares are monthly zonal mean zonal wind for December at 45°N (top panel) and for June at 35°S (bottom panel). The dashed line is the best-fitting statistical model curve calculated from Eq. (1) including the autoregressive error term.

autoregressive error term (dashed lines) are compared to the observationally derived zonal wind values at 45°N in December and at 35°S in June. Considerable year-to-year variability is present (part of which is attributable to the QBO) and the relationship is not as good at 35°S as at 45°N. However, a long-term variation that is in approximate phase with the solar cycle can be seen in both the NH and SH cases.

Figure 7 shows solar regression coefficients for the 2-mb level (1–2 mb in the case of ozone). A low-latitude band of positive ozone response is present in the top panel (a) along with a number of positive maxima at high winter latitudes that are significant at the 2σ level. As shown in the center panel, temperature maxima also occur at high winter latitudes that are inversely correlated with the ozone maxima (see next section). At low latitudes, the large temperature response maximum seen at 1 mbar has nearly disappeared except for a few marginally significant islands of response. As shown in the lower panel, the December wind maximum is still present with slightly diminished amplitude, but the June/July maximum has weakened and is only marginally significant. Bands of negative response are centered mainly on the spring and summer hemispheres. It should be noted that the temperature perturbation anomalies of Fig. 7b tend to be located just north and south of the locations of the December and June/July wind maxima of Fig. 5c. This will be interpreted in terms of an associated mean meridional circulation in section 5c.

Figure 8 shows solar regression coefficients for the 5-mb level (2–4 mb in the case of ozone). The low-latitude ozone response is weaker at this level but high-

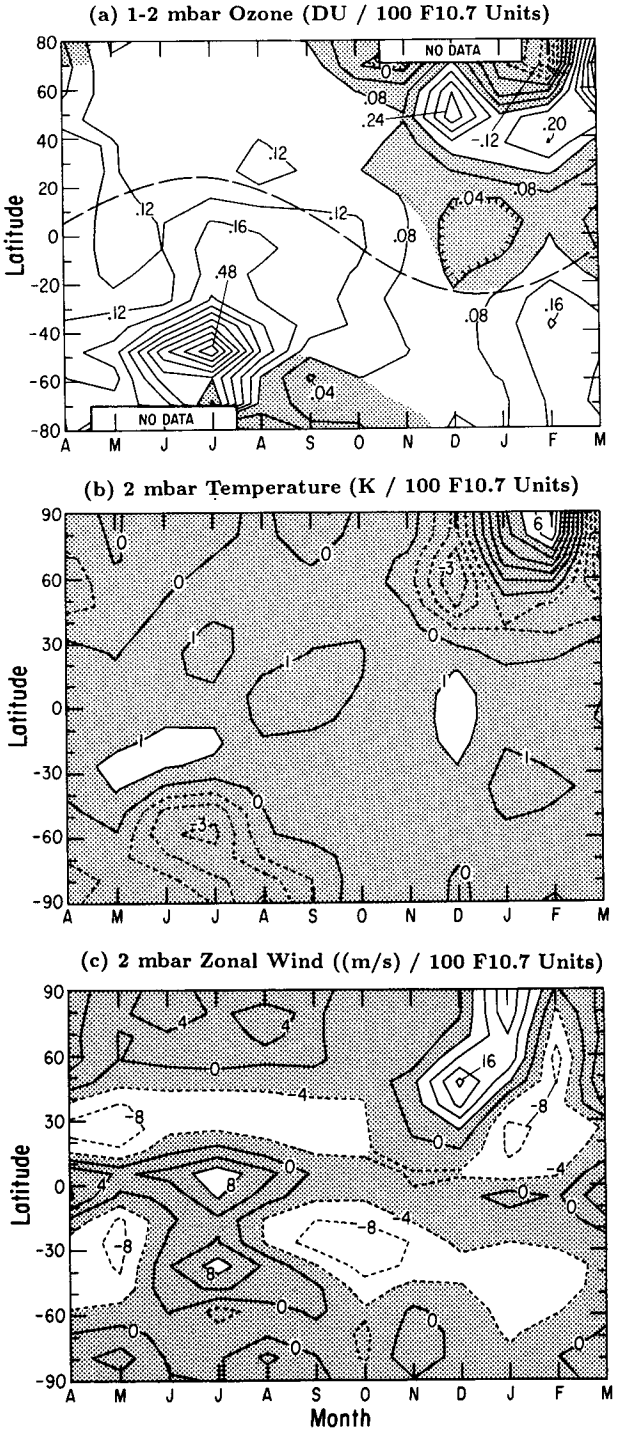

FIG. 7. Same format as Fig. 5 but for the layer 1–2 mb (ozone) and for the 2-mb level (temperature and zonal wind). The long-dashed line in the top panel is the line of zero solar zenith angle. Shaded regions are not statistically significant at the 2σ level.

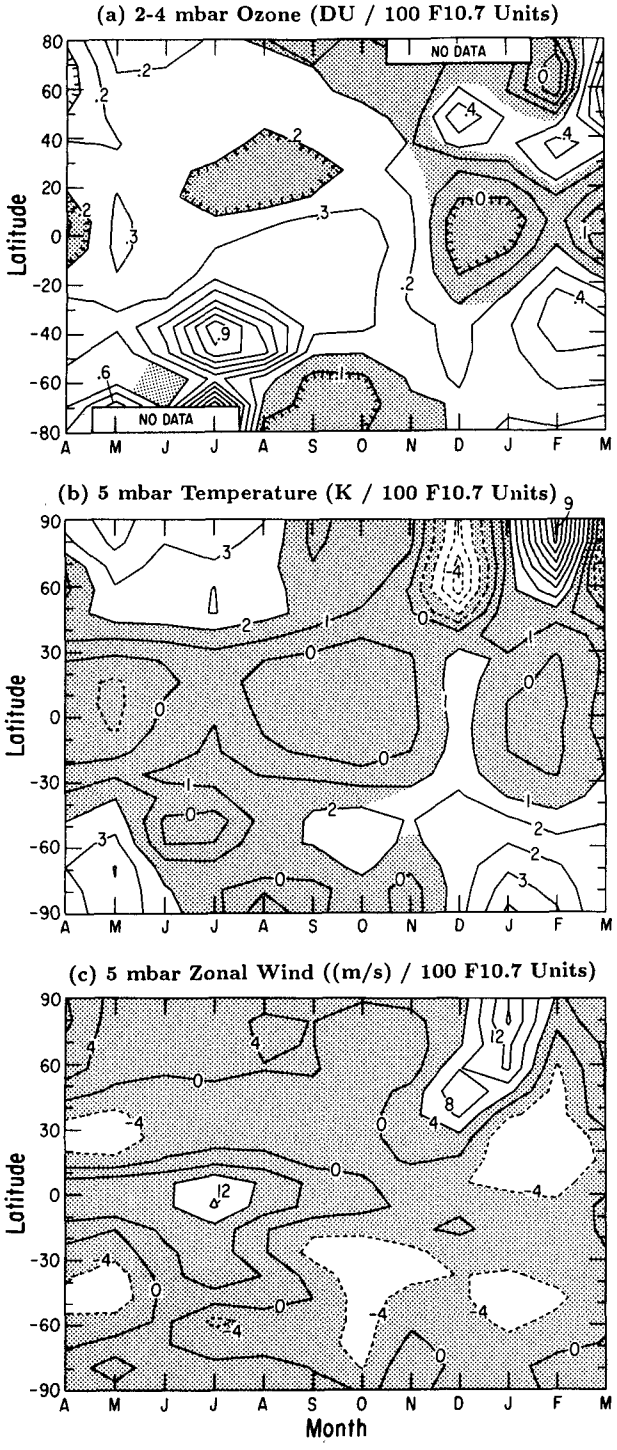

FIG. 8. Same format as Fig. 5 but for the layer 2–4 mbar (ozone) and for the 5-mb level (temperature and zonal wind). Shaded regions are not statistically significant.

latitude maxima continue to be present. As shown in the center panel, a dipolar temperature response bracketing the December wind maximum continues to be present. A large (~9 K/100 F10.7 units) maximum has appeared in February at high northern latitudes. As shown in the lower panel, the December wind maximum is reduced to an amplitude of ~10 m s^{-1}, but a second maximum has appeared at high latitudes in January. Near the equator in July, a maximum of ~12 m s^{-1} has become significant at the 2σ level.

By 10 mb (Fig. 9c), the December wind maximum is no longer detectable but the January high-latitude maximum continues to be apparently significant. The tropical wind coefficient maximum in July is reduced in amplitude. The temperature coefficient map at 10 mbar (Fig. 9b) shows several negative low-latitude anomalies in agreement with the annual average coefficients in the bottom panel of Fig. 4. Several high-latitude temperature coefficient maxima in the northern winter appear to be associated with the January wind coefficient maximum. Finally, the ozone coefficient map at 4–8 mb shows several maxima at low latitudes in the SH winter whose relationship, if any, to the temperature and wind coefficients is unclear.

5. Interpretation

Several characteristics of the observed ozone, temperature, and zonal wind interannual variations in the upper stratosphere during the ~12-year analysis period are consistent with solar cycle effects of ultraviolet radiation variations. First, the nearly globally averaged SBUV ozone and NMC temperature data near the stratopause (Fig. 1) both exhibit an apparent solar cycle variation that is qualitatively consistent with increases in the photochemical production rate of ozone and with increases in solar radiative heating between solar minimum and maximum. Second, multiple regression statistical analysis near 1 mb (top panels of Figs. 3 and 4) yields significantly positive annual mean solar regression coefficients for both ozone and temperature at low latitudes. This low-latitude response is qualitatively expected for radiative and photochemical forcing. Third, the largest positive zonal wind solar regression coefficients at 1 mb (Fig. 5c) occur at or near the extrema of the annual cycle for winter westerlies in both the Northern and Southern hemispheres. This characteristic is qualitatively consistent with solar radiative forcing since the latitudinal gradient of solar radiative heating (and, hence, zonal mean thermal wind) reaches a maximum under winter solstice conditions.

On the other hand, a number of quantitative characteristics of the derived ozone, temperature, and zonal wind solar coefficients are quite different from the predictions of current stratospheric models. Most obviously, the derived ozone, temperature, and winter solstice wind solar regression coefficients at 1 mb are significantly larger than expected theoretically for currently accepted limits on the solar cycle change in solar spectral irradiance. In the remainder of this section,

we consider these quantitative differences in more detail and discuss possible interpretations.

a. *Comparisons with radiative and photochemical models*

Even at low latitudes, the altitude dependences of the derived ozone and temperature annual mean solar regression coefficients are different from the predictions of radiative photochemical models. Specifically, as shown in Figs. 10 and 11, both the observed ozone and temperature solar cycle changes are larger near the stratopause than model predictions but are smaller and even negative at lower levels. Figure 10 compares the SBUV ozone variation over the last solar cycle at 5°N (assuming a peak-to-peak change in F10.7 of 130 flux units) with model predictions that incorporate approximately the observed change in solar spectral irradiance. The observationally estimated SBUV ozone change over a solar cycle (from Fig. 3) is shown as a percentage change calculated by dividing the regression coefficients by the long-term mean ozone column amount at 5°N in each layer. The latter amounts are approximately 0.9 DU in the 0.5–1-mb layer, 2.6 DU in the 1–2-mb layer, 10.5 DU in the 2–4-mb layer, and 28 DU in the 4–8-mb layer. The model curve in Fig. 10 is the result of a two-dimensional calculation by Brasseur et al. (1988) that adopted a solar flux change from solar minimum to maximum of 9% at 205 nm and 4% at 210–250 nm. This model is representative of other comparable simulations (Wuebbles et al. 1991; C. Jackman, personal communication). At 1 mb, the estimated ozone change is approximately twice as large as the model prediction while at lower levels, the ozone change is smaller than predicted theoretically, becoming significantly negative at the two lowest sampled levels.

In Fig. 11, the derived NMC temperature variation at 5°N over a solar cycle is seen to be largest near the stratopause (~5 K) but decreases rapidly with decreasing altitude, becoming negative at 10 mb. In order to compare these observationally derived estimates with theoretical expectations, it is useful to consider a simplified radiative equilibrium temperature model based essentially on the parameterized ozone heating model of Strobel (1978). Nominal atmospheric densities and temperatures are obtained from the climatology of Fleming et al. (1988); ozone mixing ratios and column densities at a given level are obtained from the climatology of Keating and Young (1985). Because the diurnally averaged heating rate in the upper stratosphere is mainly due to O_3 absorption in the Hartley region (242–278 nm) and Huggins bands (278–360 nm), heating rate changes over a solar cycle can occur as a result of variations in ozone concentration, variations of UV flux near 240 nm, or both. We have used the observed ozone percentage changes of Fig. 10 in calculating the solar cycle change of radiative heating.

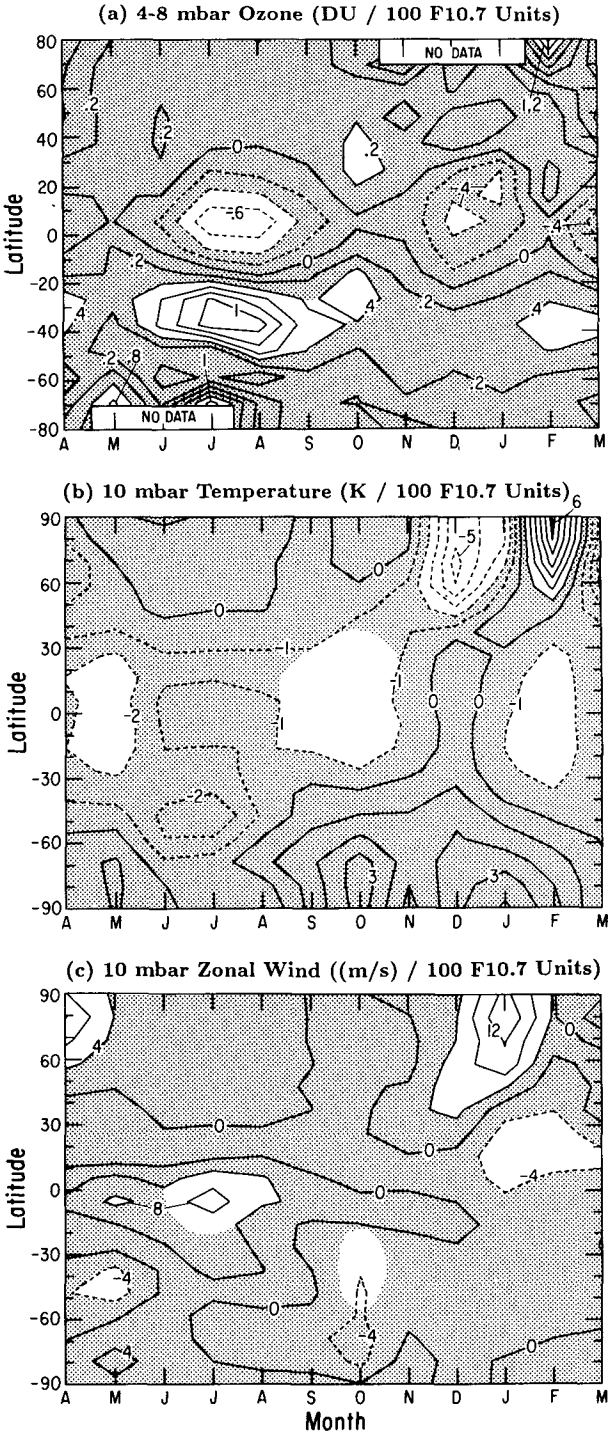

FIG. 9. Same format as Fig. 5 but for the layer 4–8 mbar (ozone) and for the 10-mb level (temperature and zonal wind). Shaded regions are not statistically significant.

This is done for both the ozone mixing ratio at a given level (which increases the heating rate from solar minimum to maximum) and for the ozone column above that level (which slightly decreases the heating rate).

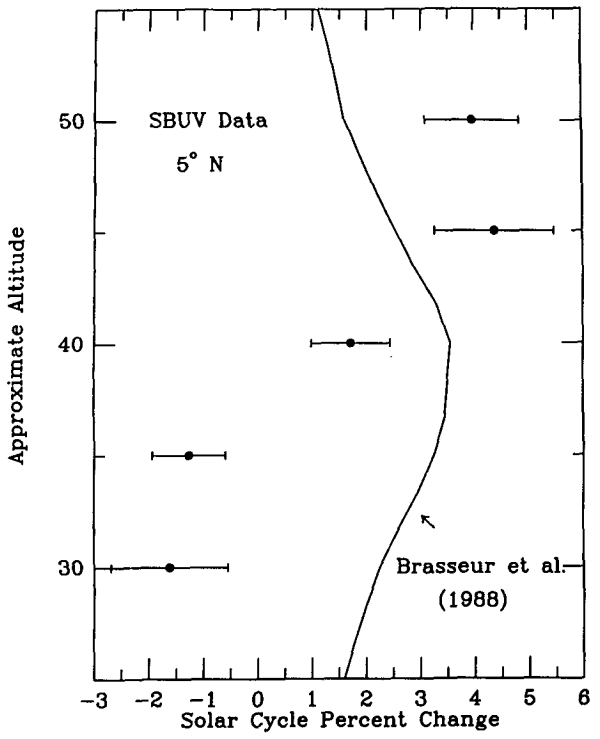

FIG. 10. Comparison of observationally derived ozone change over the last solar cycle at 5°N (solid circles) to that predicted by a two-dimensional stratospheric model (solid line). The data values were calculated from the regression results of Fig. 3 assuming a solar cycle change of 130 units of F10.7. The model calculation assumed a solar cycle change in solar flux at 205 nm of 9%, which is within the range allowed by current solar spectral irradiance data.

For the UV solar spectral irradiance change over a solar cycle, a variation of 9% at 205 nm was assumed with corresponding changes at other wavelengths estimated from the 27-day measurements of Donnelly (1988). For these UV and ozone changes, the Strobel parameterization yields a solar cycle change in the total diurnally averaged heating rate near 1 mbar of about 4% or $\sim$0.4 K day^{-1}. Radiative cooling is approximated using a latitudinally constant Newtonian cooling profile (e.g., Schoeberl and Strobel 1978). The radiative equilibrium temperature at a given level and latitude is then estimated from $T_{eq} = T_{ref} + \tau_N(h - h_{ref})$, where T_{ref} and h_{ref} are the observed climatological temperature and calculated reference heating rate at some reference latitude where radiative equilibrium is a good approximation (taken here to be the equator), h is the calculated heating rate at a given latitude, and τ_N is an effective Newtonian cooling lifetime. The model curve in Fig. 11 is the solar cycle change in radiative equilibrium temperature at 5°N calculated from this simple model. The maximum temperature change is slightly under 2 K near 45 km. Despite the simplicity of the model, this result is in reasonable agreement with results of more complete and accurate radiative codes.

Given that the model curve of Fig. 11 is approximately valid under radiative equilibrium conditions, then it is clear that the observationally estimated temperature change $\sim$ 5 K at 1 mb over the last solar cycle is not a consequence of radiative heating changes alone. For Newtonian cooling lifetimes of $\sim$5 days near the stratopause, a solar cycle radiative heating change of $\sim$1 K day^{-1} would be required to explain the estimated temperature change in terms of radiative processes alone. Such a radiative heating rate change would require UV flux changes of more than 20% near 205 nm, which can be observationally excluded. If photochemical acceleration of the radiative relaxation lifetimes in the upper stratosphere is considered, the required radiative heating changes are even larger. A dynamical heating component of the temperature change is therefore required (see section 5c). This result may be consistent with previous theoretical suggestions that the tropical atmosphere responds relatively less to radiative forcing and more to dynamic forcing than does the extratropical atmosphere (Fels et al. 1980; Geller et al. 1992).

b. The winter solstice wind variation

In order to allow a semiquantitative discussion of the winter solstice midlatitude wind variation, it is use-

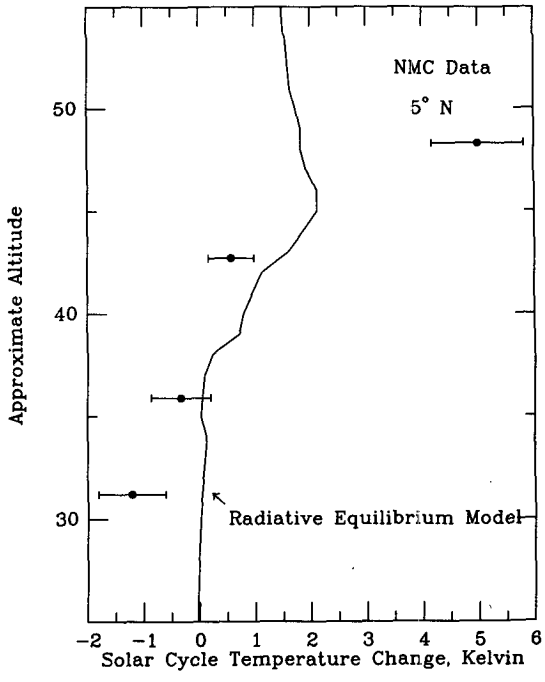

FIG. 11. The solid curve is the solar cycle temperature change at 5°N calculated from a simplified radiative equilibrium temperature model. The change in solar flux at 205 nm from solar minimum to maximum was assumed to be 9% and the ozone mixing ratio and column density change corresponded to the observational percentage changes shown in Fig. 10. The solid circles and error limits are the same as those shown in Fig. 4 for 5°N scaled to a solar cycle change in F10.7 of 130 units.

ful to consider a highly simplified but analytic model of middle atmospheric circulation described by Barnes (1991). In this model [which is based on the more detailed numerical model of Holton (1982)], a quasigeostrophic zonal mean flow on a midlatitude beta plane is calculated under the assumption that a single gravity wave mode interacts one-dimensionally with the flow that would occur under radiative equilibrium conditions. Although several approximations were introduced, Barnes found that the model yields midlatitude wind profiles that agree reasonably well with those obtained numerically using more rigorous models. The starting point is the set of quasigeostrophic transformed Eulerian mean equations on a beta plane that, in the notation of Andrews et al. (1987), are

$$\bar{u}_t - f_0\bar{v}^* = \bar{G} \tag{2}$$

$$\bar{T}_t + N^2HR^{-1}\bar{w}^* = -\alpha[\bar{T} - T_r(y, z, t)] \tag{3}$$

$$\bar{v}^*_y + \rho_0^{-1}(\rho_0\bar{w}^*)_z = 0 \tag{4}$$

$$f_0\bar{u}_z + H^{-1}R\bar{T}_y = 0, \tag{5}$$

where $\bar{u}$ is zonal mean zonal wind, $\bar{v}^*$ and $\bar{w}^*$ are the northward and upward components of a residual mean meridional circulation, $\bar{T}$ is zonal mean temperature, $\bar{G}$ is the zonal wind acceleration due to wave–mean flow interactions, ρ_0 is basic-state mass density, f_0 is the Coriolis parameter evaluated at the center of the beta-plane channel, N is the buoyancy frequency, H is a mean scale height, R is the dry air gas constant, and the subscripts y, z, and t indicate derivatives. On the right side of (3), the diabatic heating rate per unit mass has been parameterized in terms of $\bar{T}$ using a Newtonian cooling rate α and T_r, the radiative equilibrium temperature. Combining (2)–(5) yields a single equation describing the midlatitude zonal wind dependence on meridional coordinate y and altitude z [see also Eq. (7.2.11) of Andrews et al. 1987],

$$(\bar{u}_{yy})_t + \frac{f_0^2}{N^2}\left\{\alpha[\bar{u}_{zz} - (u_r)_{zz}] + (\bar{u}_{zz})_t - \frac{\alpha}{H}[\bar{u}_z - (u_r)_z] - \frac{1}{H}(\bar{u}_z)_t\right\} = \bar{G}_{yy}, \tag{6}$$

where $u_r = u_0 + (-R/f_0H)\int_{z_0}^{z}(\bar{T}_r)_y dz$ is the mean zonal wind that would exist under radiative equilibrium conditions. (Essentially u_r is the result of applying the thermal wind equation to the radiative equilibrium temperatures.) To reduce the problem to one dimension, the y dependence of $\bar{u}$, u_r, and $\bar{G}$ is assumed to be $\sin ly$ where $l = \pi/L_y$, with L_y the width of the beta channel. Further assuming a steady state and that $(u_r)_z$ is constant with height, one obtains

$$H\bar{u}_{zz} - \bar{u}_z + (u_r)_z = -\frac{l^2N^2H}{\alpha f_0^2}\bar{G}. \tag{7}$$

In order to proceed further, the wave drag and diffusion function $\bar{G}$ must be specified. Lindzen (1981) has argued that gravity wave breaking can generate convective turbulence that would lead to a net zonal drag force at mesospheric levels. On this basis, he derived a parameterization of wave stress and diffusion in terms of the zonal mean zonal wind valid for levels between the "breaking" level and the critical level where $\bar{u}$ equals the wave phase speed. The breaking level z_b is defined to be that level where a vertically propagating gravity wave "saturates," that is, where the local temperature lapse rate becomes superadiabatic allowing convective turbulence to limit the growth of the wave with height. According to Holton (1982), this level is given by

$$z_b = 3H\ln\left(\frac{|\bar{u} - c|}{\tilde{u}}\right), \tag{8}$$

where c is the wave zonal phase speed and $\tilde{u}$ is proportional to the amplitude B of the wave vertical velocity at some lower boundary z_0,

$$\tilde{u} = [BN/(k|u_0 - c|^{1/2})]^{2/3} \tag{9}$$

in which k is the zonal wavenumber and $u_0 = \bar{u}(z_0)$. However, the Lindzen–Holton parameterization of $\bar{G}$ is nonlinear in $\bar{u}$ and therefore does not allow an analytic solution of (7). A modified approximate parameterization suggested by Barnes assumes that the critical level is located one scale height above z_b and that $\bar{G}$ falls off exponentially below z_b. With these simplifications, the Lindzen–Holton parameterization reduces to

$$\bar{G} = -\left(\frac{2\gamma k\tilde{u}^3}{NH}\right)e^{z/H}, \tag{10}$$

where the e-folding decay height for $\bar{G}$ has been set equal to the atmospheric scale height H. Substituting (10) into (7), an analytic solution of (7) is obtained as

$$\bar{u}_z = a_1e^{z/H} + (u_r)_z z + Cze^{z/H} + a_2, \tag{11}$$

where $C = (2\gamma k\tilde{u}^3l^2N)/(\alpha f_0^2)$. The coefficients a_1 and a_2 are determined from boundary conditions that are taken as $\bar{u}_z(z = z_0) = \bar{u}_0$ and $\bar{u}(z = z_b + H) = c$.

Barnes (1991) showed that in the above model, the strength of the calculated zonal flow (and the height of the wind maximum) depends essentially on the ratio of the radiative forcing to the gravity wave flux. Stronger radiative forcing leads to stronger flows and higher gravity wave breaking levels, while stronger wave flux (incident from the troposphere) leads to weaker flows and lower breaking levels. Because radiative forcing is a maximum at winter solstice while tropospheric wave forcing is relatively constant with season, westerly wind maxima are expected under winter solstice conditions. The solid line labeled "winter solstice" in Fig. 12 plots the solution (11) for the nominal winter parameters listed in appendix B of Barnes (1991). To estimate the

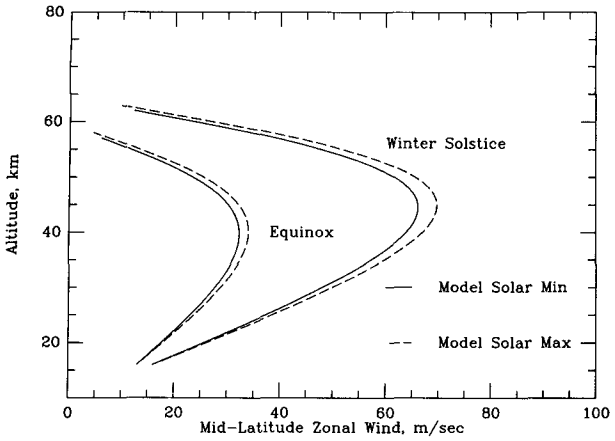

FIG. 12. The solid lines are midlatitude zonal wind profiles for equinox (March) and winter solstice (December) conditions calculated from the analytic model of Barnes (1991) with radiative equilibrium zonal wind shears appropriate for solar minimum conditions (see the text). The dashed lines are for radiative equilibrium zonal wind shears appropriate for solar maximum conditions assuming a 3% increase in ozone mixing ratio at all levels.

radiative forcing, we have calculated $(u_r)_z$ using the simplified radiative equilibrium temperature model described above, obtaining for winter solstice conditions at 45°N and ~45 km altitude, $(u_r)_z = 2.54$ m s^{-1} km. For equinox (March) conditions, the radiative equilibrium model yields a reduced radiative equilibrium wind shear at 45°N of 1.27 m s^{-1}/km. The solid line labeled "equinox" in Fig. 12 plots the solution (11) for this reduced radiative forcing. The calculated December and March peak wind amplitudes near 1 mbar are in reasonable agreement with the observed long-term means in Fig. 2c.

The dashed lines in Fig. 12 illustrate the effect of adding an upper-limit solar cycle increase in radiative heating on the zonal wind profiles calculated from the Barnes (1991) model. Specifically, the solar flux at 205 nm was assumed to have increased by 9% with corresponding increases at other wavelengths; the concentration of stratospheric ozone was assumed to have increased by 3% at all levels and latitudes, while the ozone column was artificially held constant. The resulting upper bound values of the radiative equilibrium wind shear at 45°N in December and March were 2.68 m s^{-1}/km and 1.35 m s^{-1}/km, respectively. As shown in Fig. 12, the winter solstice zonal wind amplitude increased by nearly 5 m s^{-1}, while the equinox wind was increased by about 2 m s^{-1}. Although the larger wind increase at winter solstice is qualitatively consistent with the observed solar coefficients of Fig. 5c, the amplitude is much less than that derived observationally. In particular, according to Fig. 5c, the observed December northern midlatitude wind increase from solar minimum to maximum during the last solar cycle was 23 ± 9 m s^{-1}, while that in June/July at southern midlatitudes was 18 ± 16 m s^{-1} (assuming 130 flux units of change in F10.7). Thus, radiative forcing alone is not an adequate explanation for the observed winter solstice midlatitude wind changes.

In order to generate the full amplitude of the winter solstice wind increases over the last solar cycle using the Barnes model, it is necessary to change the magnitude of the wave forcing function $\bar{G}$ as well as that of the radiative forcing. The possibility that wave forcing is an inherent part of the winter solstice wind variation is suggested also by the greater amplitude of the wind change in the NH (where wave activity is stronger) than in the SH. Trial calculations indicate that a reduction in the effective magnitude of $\bar{G}$ by a factor of ~6 would be sufficient to increase the winter solstice wind amplitude at 1 mb by about 20 m s^{-1}. However, as reviewed in section 2, planetary-scale Rossby waves are believed to be principally responsible for wave driving of upper-stratospheric winter climatology. Rossby waves propagate meridionally as well as vertically and travel along ray paths that are sensitive to spatial variations in the effective refractive index governing wave propagation. Since these waves both determine the flow and are affected by the flow, an external perturbation such as solar ultraviolet variations may produce larger wind variations than would be predicted by simple linear models. Hence, the analytic dynamical model considered here in which a single vertically propagating gravity wave mode determines the circulation is probably too simple for further diagnosis purposes. Future theoretical comparisons must employ a more complete numerical model of planetary wave propagation and interactions with the mean flow; in addition, multiple regression statistical studies of wave properties (Eliassen–Palm flux, flux divergence, wave one amplitude, etc.) using Randel's (1992) circulation statistics would provide some useful additional constraints.

c. *Associated residual meridional circulation*

As reviewed in section 2, a residual poleward meridional circulation exists in the winter upper stratosphere that is driven by deceleration of the mean zonal flow resulting from planetary wave drag and diffusion. This residual circulation results in a net downwelling near the winter pole that heats the winter polar upper stratosphere to temperatures well above that expected from radiative equilibrium calculations. As concluded in the previous subsection, the increased winter solstice zonal wind amplitudes near the stratopause at solar maximum require a reduced wave drag function $\bar{G}$. Consequently, the poleward winter meridional circulation in the upper stratosphere is expected to be reduced near solar maximum as compared to solar minimum. The reduction of the poleward meridional circulation associated with the NH winter solstice wind acceleration is indicated empirically in Figs. 7b and 8b by the occurrence of positive and negative temperature

extrema to the north and south of the December wind maxima of Figs. 5c and 7c. A second pair of such extrema is also present in the SH in June and July at 2 mb (Fig. 7b). These temperature anomalies are consistent with decreased adiabatic cooling at low latitudes and heating at high latitudes, implying reduced upwelling at low latitudes and reduced descending motions at higher latitudes. By mass continuity, these vertical velocity components at low and high latitudes are in turn consistent with a reduced poleward meridional flow at middle latitudes associated with the zonal wind increase from solar minimum to maximum.

An approximate estimate for the low-latitude temperature perturbation produced by the net reduction of the poleward meridional circulation between solar minimum and maximum can be obtained from the analytic model discussed in the previous subsection. At 48 km, the gravity wave drag and diffusion term $\bar{G}$ has an amplitude of -6.95 m s^{-1} per day for the nominal winter case of Barnes (1991). In order to allow an $\sim$ 20 m s^{-1} increase of the wind amplitude, $\bar{G}$ must be decreased to about -1.25 m s^{-1} per day. According to (2) in a steady state, $\bar{v}^* \approx -\bar{G}/f_0$. For $f_0 = 8.6$ day^{-1}, the implied meridional velocity change between solar minimum and maximum is $\Delta\bar{v}^* \approx -0.66$ m s^{-1}. From (4), if $\bar{w}^*$ does not change too rapidly over a scale height, then at low latitudes, $\bar{w}^* \approx H/\Delta\bar{v}^*$ or $\bar{w}^* \approx -2.2 \times 10^{-3}$ m s^{-1}. From (3), the implied adiabatic temperature change is approximately $-(N^2H/R\alpha)\bar{w}^*$. For nominal parameters, the resulting estimated temperature increase at low latitudes from solar minimum to maximum is $\sim$5 K. As concluded in section 5a, the observed low-latitude temperature variation over the last solar cycle near 1 mb requires a dynamical heating component in addition to radiative forcing. The agreement in order of magnitude of the temperature perturbation at low latitudes expected from the net reduction of the poleward mean meridional circulation with the low-latitude temperature increases at 1 mb shown in Figs. 4a and 5b suggests that such a net meridional circulation change in both hemispheres may explain the large amplitudes of the 1-mb solar cycle temperature variation.

The associated meridional circulation change between solar minimum and maximum in both hemispheres under winter solstice conditions may also explain the existence of several of the high-latitude winter ozone extrema evident in Figs. 5a, 7a, and 8a. Since ozone is nearly in photochemical equilibrium in the upper stratosphere, positive temperature deviations produce negative ozone deviations and vice versa. Many of the NH ozone extrema in December and the SH ozone extrema in June and July correlate with temperature extrema of opposite sign induced by the meridional circulation. In addition, the unexpectedly high amplitude of the upper-stratospheric solar cycle ozone change at low latitudes (Fig. 10) may also be driven, at least in part, by the net meridional circulation change. Although ozone is nearly in photochemical equilibrium, advective transport terms can still be significant, especially in the winter upper stratosphere (e.g., Douglass and Rood 1986). Since the winter ozone concentration at 1 mbar increases with latitude (Fig. 2a), a reduction of the net poleward meridional circulation between solar minimum and maximum would result in less meridional transport of ozone away from the low-latitude production region. The result would be enhanced ozone concentrations at low latitudes at solar maximum compared to that at solar minimum.

6. Discussion and conclusions

Although available satellite remote sensing datasets are temporally limited, the existing measurements are consistent with a significant solar cycle variation of upper-stratospheric ozone and temperature at low latitudes and of winter solstice zonal wind at middle latitudes in both hemispheres. Since ozone and temperature are independently measured, the observed variation in phase with long-term solar ultraviolet variations as represented by F10.7 (Fig. 1) is unlikely to be fortuitous despite the short record length (slightly more than one solar cycle). The occurrence of both ozone and temperature increases at low latitudes from solar minimum to maximum at 1 mbar is supportive of an origin involving photochemical and radiative effects of solar cycle changes in ultraviolet radiation. The major alternative of an internal dynamical variation with a period $\sim$10 years can be excluded since the resulting temperature variation near the stratopause would drive ozone variations of opposite sign, unlike the in-phase variation of both ozone and temperature that is seen in Fig. 1. The occurrence of winter solstice wind increases from solar minimum to maximum at 1 mbar at middle latitudes is qualitatively consistent with solar ultraviolet forcing, as evidenced by simplified model calculation results such as those of Fig. 12. Finally, the occurrence of winter solstice wind enhancements near the midlatitude stratopause in the SH as well as in the NH reduces the likelihood that the solar-correlated December wind enhancement originally reported by Kodera and Yamazaki (1990) is an accident of the limited temporal record length.

Comparisons with model calculations indicate that the low-latitude ozone and temperature variations at 1 mbar over the last solar cycle were both in excess of predictions based on photochemical and radiative heating effects alone (Figs. 10 and 11). A significant dynamically forced component of the stratopause ozone and temperature responses is therefore needed if the observed interannual variations are to be solar induced. The midlatitude zonal wind variation from solar minimum to maximum near the winter solstice stratopause (December in the NH and June/July in the SH) has an amplitude that is larger by a factor of at least 4 than expected from model calculations that

consider radiative forcing alone together with observed solar cycle changes in solar ultraviolet spectral irradiance. If the December zonal wind variation is solar forced, then a positive feedback process involving solar cycle variations of wave driving is required such that the effective deceleration of the stratopause zonal wind by wave–mean flow interactions is increased under solar minimum conditions. The importance of wave driving in determining the winter solstice wind variation is also suggested by the observed higher amplitude of the NH December wind variation relative to the SH June/July wind variation at 1 mbar. A net reduction of the poleward residual mean meridional circulation is associated with the winter solstice midlatitude zonal wind increase from solar minimum to maximum. Dipolar pairs of solar cycle temperature variations exist at lower levels to the north and south of the winter solstice wind peak in both hemispheres, consistent with such a circulation change. Approximate calculations (section 5c) indicate that this net meridional circulation change may result in reduced adiabatic cooling at low latitudes and reduced poleward meridional transport of ozone. These secondary transport effects in both hemispheres could then contribute to the unexpectedly high amplitudes of the temperature and ozone solar cycle variation at 1 mbar at low latitudes.

An important issue left unresolved by the present study is the nature of the positive feedback process involving wave–mean flow interactions that appears to amplify the radiatively forced zonal wind variation near the winter solstice stratopause. Several theoretical studies have previously indicated that relatively modest changes in the radiation treatment can sometimes lead to unexpectedly large changes in zonal wind and temperature (e.g., Ramanathan et al. 1983). An example of a different middle atmospheric perturbation whose origin also requires positive feedback due to wave–mean flow interaction is the extratropical zonal wind QBO (Holton and Tan 1982; Dunkerton and Baldwin 1991). The primary tropical QBO apparently induces detectable effects on a variety of extratropical phenomena including the occurrence of major midwinter warmings (e.g., Labitzke 1982), the interannual variability of total ozone (e.g., Bowman 1989), and the depth of the springtime Antarctic ozone depletion (e.g., Lait et al. 1989). However, current numerical models of middle atmospheric circulation have not yet fully determined the nature of the wave–mean flow feedbacks that lead to these extratropical effects (e.g., Holton and Austin 1991). Recent observational efforts to constrain the origin of the extratropical QBO have concentrated on the analysis of planetary wave statistics such as Eliassen–Palm flux and flux divergence (Dunkerton and Baldwin 1991). Similar analyses can in principle be carried out for the stratopause wind variation studied here now that more than one solar cycle of wave statistics are available. The results of this study indicate that such analyses are required for a better understanding of the upper-stratospheric response to solar cycle changes in ultraviolet radiation.

While more definitive results will undoubtedly be obtained when additional solar cycles of upper-stratospheric remote sensing measurements are acquired, it should be stated that the current results are supportive of possible secondary or derivative effects of solar cycle ultraviolet forcing at lower levels in the stratosphere and upper troposphere. As shown by Kodera et al. (1990), derivative effects of the December wind variation occur later in the northern winter. Manifestations of these derivative effects probably include the January and February wind, temperature, and ozone solar coefficient extrema evident at high northern latitudes in Figs. 5, 7, 8, and 9. Similar derivative effects may occur at lower levels and in other seasons [for example, see Kodera et al. (1991b)]. The correlative results of Labitzke and van Loon (1988) and van Loon and Labitzke (1990) may therefore be ultimately understood as resulting essentially from dynamical effects of solar ultraviolet variations on the upper stratosphere.

Acknowledgments. We are indebted to W. Randel of NCAR for help in accessing his atmospheric circulation statistics dataset, which includes the NOAA NMC data; to M. Gelman of the NMC Climate Analysis Center, who supplied updated adjustment coefficients for the NMC temperature data prior to publication; and to R. D. McPeters of Goddard Space Flight Center, who provided monthly zonal means of the reprocessed (Version 6) SBUV ozone measurements. Thanks are also due to J. Angell for providing the 30-mb Singapore zonal wind data and to M. Baldwin and T. Dunkerton for preliminary discussions of the NMC data. Supported by NSF Grant ATM9012012 and NASA Grant NAGW-909.

REFERENCES

Andrews, D. G., J. R. Holton, and C. B. Leovy, 1987: *Middle Atmosphere Dynamics.* Academic Press, 489 pp.

Angell, J. K., 1991: Stratospheric temperature change as a function of height and sunspot number during 1972–89 based on rocketsonde and radiosonde data. *J. Climate,* **4,** 1170–1180.

Baldwin, M. P., and T. J. Dunkerton, 1989: Observations and statistical simulations of a proposed solar cycle/QBO/weather relationship. *Geophys. Res. Lett.,* **16,** 863–867.

——, and ——, 1991: Quasi-biennial oscillation above 10 mb. *Geophys. Res. Lett.,* **18,** 1205–1208.

Barnes, J. R., 1991: A simple nearly analytic model of a gravity wave driven middle atmosphere circulation. *J. Atmos. Sci.,* **48,** 225–235.

Bowman, K. P., 1989: Global patterns of the quasi-biennial oscillation in total ozone. *J. Atmos. Sci.,* **46,** 3328–3343.

Brasseur, G., and S. Solomon, 1984: *Aeronomy of the Middle Atmosphere.* D. Reidel, 441 pp.

——, M. H. Hitchman, P. C. Simon, and A. De Rudder, 1988: Ozone reduction in the 1980's: A model simulation of anthropogenic and solar perturbations. *Geophys. Res. Lett.,* **15,** 1361–1364.

Callis, L. B., J. C. Alpert, and M. A. Geller, 1985: An assessment of thermal, wind, and planetary wave changes in the middle and lower atmosphere due to 11-year UV flux variations. *J. Geophys. Res.,* **90,** 2273–2282.

Cebula, R. P., M. T. DeLand, and B. M. Schlesinger, 1992: Estimates of solar variability using the Mg II index from the *NOAA-9* satellite. *J. Geophys. Res.*, **97,** 11 613–11 620.

Chandra, S., 1986: The solar and dynamically induced oscillations in the stratosphere. *J. Geophys. Res.*, **91,** 2719–2734.

——, 1991: The solar UV related changes in total ozone from a solar rotation to a solar cycle. *Geophys. Res. Lett.*, **18,** 837–840.

Donnelly, R. F., 1988: Uniformity in solar UV flux variations important to the stratosphere. *Ann. Geophys.*, **6,** 417–424.

——, 1991: Solar UV spectral irradiance variations. *J. Geomagn. Geoelect.*, **43**(Suppl., Part 2), 835–842.

——, D. F. Heath, J. L. Lean, and G. J. Rottman, 1983: Differences in the temporal variations of solar UV flux, 10.7-cm solar radio flux, sunspot number, and Ca-K plage data caused by solar rotation and active region evolution. *J. Geophys. Res.*, **88,** 9883–9888.

Douglass, A. R., and R. Rood, 1986: Derivation of photochemical information near 1 mbar from ozone and temperature data. *J. Geophys. Res.*, **91,** 13 153–13 166.

Dunkerton, T. J., and M. P. Baldwin, 1991: Quasi-biennial modulation of planetary-wave fluxes in the Northern Hemisphere winter. *J. Atmos. Sci.*, **48,** 1043–1061.

——, and ——, 1992: Modes of interannual variability in the stratosphere. *Geophys. Res. Lett.*, **19,** 49–52.

Fels, S. B., 1985: Radiative–dynamical interactions in the middle atmosphere. *Advances in Geophysics,* Vol. 28A, Academic Press, 277–300.

——, J. D. Mahlman, M. D. Schwarzkopf, and R. W. Sinclair, 1980: Stratospheric sensitivity to perturbations in ozone and carbon dioxide: Radiative and dynamical response. *J. Atmos. Sci.*, **37,** 2265–2297.

Finger, F. G., M. E. Gelman, J. D. Wild, M. L. Chanin, A. Hauchecorne, and A. J. Miller, 1993: Evaluation of NMC upper stratospheric analyses using rocketsonde and lidar data. *Bull. Amer. Meteor. Soc.*, **74,** 789–799.

Fleming, E. L., S. Chandra, M. R. Schoeberl, and J. J. Barnett, 1987: Monthly mean global climatology of temperature, wind, geopotential height, and pressure for 0–120 km. NASA Tech. Memo. 100697, 85 pp.

Frederick, J. E., F. T. Huang, A. R. Douglass, and C. A. Reber, 1983: The distribution and annual cycle of ozone in the upper stratosphere. *J. Geophys. Res.*, **88,** 3819–3828.

Geller, M., E. R. Nash, M. F. Wu, and J. E. Rosenfield, 1992: Residual circulations calculated from satellite data: Their relations to observed temperature and ozone distributions. *J. Atmos. Sci.*, **49,** 1127–1137.

Gelman, M. E., A. J. Miller, R. M. Nagatani, and H. D. Bowman II, 1983: Mean zonal wind and temperature structure during the PMP-1 winter periods. *Adv. Space Res.*, **2,** 159–162.

——, ——, K. W. Johnson, and R. M. Nagatini, 1986: Detection of long-term trends in global stratospheric temperature from NMC analyses derived from NOAA satellite data. *Adv. Space Res.*, **6,** 17–26.

Gille, J. C., C. M. Smythe, and D. F. Heath, 1984: Observed ozone response to variations in solar ultraviolet radiation. *Science,* **225,** 315–317.

Heath, D. F., and B. M. Schlesinger, 1986: The Mg 280-nm doublet as a monitor of changes in solar ultraviolet irradiance. *J. Geophys. Res.*, **91,** 8672–8682.

——, A. J. Krueger, H. A. Roeder, and B. D. Henderson, 1975: The solar backscatter ultraviolet and total ozone mapping spectrometer (SBUV/TOMS) for Nimbus G. *Opt. Eng.*, **14,** 323–340.

Herman, J. R., R. Hudson, R. McPeters, R. Stolarski, Z. Ahmad, X-Y Gu, S. Taylor, and C. Wellemeyer, 1991: A new self-calibration method applied to TOMS/SBUV backscattered ultraviolet data to determine long term global ozone change. *J. Geophys. Res.*, **96,** 7531–7546.

Holton, J. R., 1982: The role of gravity wave induced drag and diffusion in the momentum budget of the mesosphere. *J. Atmos. Sci.*, **39,** 791–799.

——, and H.-C. Tan, 1982: The quasi-biennial oscillation in the Northern Hemisphere lower stratosphere. *J. Meteor. Soc. Japan,* **60,** 140–148.

——, and J. Austin, 1991: The influence of the equatorial QBO on sudden stratospheric warmings. *J. Atmos. Sci.*, **48,** 607–618.

Hood, L. L., 1984: The temporal behavior of upper stratospheric ozone at low latitudes: Evidence from *Nimbus-4* BUV data for short-term responses to solar ultraviolet variability. *J. Geophys. Res.*, **89,** 9557–9568.

——, 1986: Coupled stratospheric ozone and temperature responses to short-term changes in solar ultraviolet flux: An analysis of Nimbus 7 SBUV and SAMS data. *J. Geophys. Res.*, **91,** 5264–5276.

——, and J. L. Jirikowic, 1991: Stratospheric dynamical effects of solar ultraviolet variations: Evidence from zonal mean ozone and temperature data. *J. Geophys. Res.*, **96,** 7565–7577.

——, and J. P. McCormack, 1992: Components of interannual ozone change based on *Nimbus-7* TOMS data. *Geophys. Res. Lett.*, **19,** 2309–2312.

——, Z. Huang, and S. W. Bougher, 1991: Mesospheric effects of solar ultraviolet variations: Further analysis of SME IR ozone and Nimbus-7 SAMS temperature data. *J. Geophys. Res.*, **96,** 12 989–13 002.

Keating, G. M., and D. F. Young, 1985: Interim reference ozone models for the middle atmosphere. *Middle Atmosphere Program, Handbook for MAP, 16,* K. Labitzke, J. J. Barnett, and B. Edwards, Eds., SCOSTEP Secretariat, University of Illinois, Urbana, 205–230.

——, G. P. Brasseur, J. Y. Nicholson III, and A. De Rudder, 1985: Detection of the response of ozone in the middle atmosphere to short-term solar ultraviolet variations. *Geophys. Res. Lett.*, **12,** 449–452.

——, J. Y. Nicholson III, D. F. Young, G. Brasseur, and A. De Rudder, 1987: Response of middle atmosphere to short-term solar ultraviolet variations: 1. Observations. *J. Geophys. Res.*, **92,** 889–902.

Kodera, K., 1991: The solar and equatorial QBO influences on the stratospheric circulation during the early northern-hemisphere winter. *Geophys. Res. Lett.*, **18,** 1023–1026.

——, and K. Yamazaki, 1990: Long-term variation of upper stratospheric circulation in the northern hemisphere in December. *J. Meteor. Soc. Japan,* **68,** 101–105.

——, K. Yamazaki, M. Chiba, and K. Shibata, 1990: Downward propagation of upper stratospheric mean zonal wind perturbation to the troposphere. *Geophys. Res. Lett.*, **17,** 1263–1266.

——, M. Chiba, and K. Shibata, 1991a: A general circulation model study of the solar and QBO modulation of the stratospheric circulation during the northern hemisphere winter. *Geophys. Res. Lett.*, **18,** 1209–1212.

——, ——, K. Yamazaki, and K. Shibata, 1991b: A possible influence of the polar night stratospheric jet on the subtropical tropospheric jet. *J. Meteor. Soc. Japan,* **69,** 715–721.

Labitzke, K., 1982: On the interannual variability of the middle stratosphere during the northern winters. *J. Meteor. Soc. Japan,* **60,** 124–138.

——, and H. van Loon, 1988: Associations between the 11-year solar cycle, the QBO, and the atmosphere, Part I: The troposphere and stratosphere in the northern hemisphere in winter. *J. Atmos. Terr. Phys.*, **50,** 197–206.

Lait, L. R., M. R. Schoeberl, and P. A. Newman, 1989: Quasi-biennial modulation of the Antarctic ozone depletion. *J. Geophys. Res.*, **94,** 11 559–11 571.

Lean, J., 1991: Variations in the sun's radiative output. *Rev. Geophys.*, **29,** 505–536, 1991.

Lindzen, R. S., 1981: Turbulence and stress due to gravity wave and tidal breakdown. *J. Geophys. Res.*, **86,** 9707–9714.

McPeters, R. D., and W. D. Komhyr, 1991: Long-term changes in the Total Ozone Mapping Spectrometer relative to world primary standard Dobson spectrometer 83. *J. Geophys. Res.*, **96,** 2987–2993.

——, D. F. Heath, and P. K. Bhartia, 1984: Average ozone profiles for 1979 from the *Nimbus-7* SBUV instrument. *J. Geophys. Res.*, **89,** 5199–5214.

Neter, J., W. Wasserman, and M. H. Kutner, 1985: *Applied Linear Regression Models.* R. D. Irwin, 523 pp.

Pollack, J. B., and T. P. Ackerman, 1983: Possible effects of the El Chichon cloud on the radiation budget of the northern tropics. *Geophys. Res. Lett.*, **10,** 1057–1060.

Ramanathan, V., E. J. Pitcher, R. C. Malone, and M. L. Blackmon, 1983: The response of a spectral general circulation model to refinements in radiative processes. *J. Atmos. Sci.*, **40,** 605–630.

Randel, W. J., 1987: The evaluation of winds from geopotential height data in the stratosphere. *J. Atmos. Sci.*, **44,** 3097–3120.

——, 1992: Global atmospheric circulation statistics, 1000-1 mb. NCAR Tech. Note TN-366, National Center for Atmospheric Research, Boulder, Colorado, 256 pp.

Salby, M. L., and D. J. Shea, 1991: Correlations between solar activity and the atmosphere: An unphysical explanation. *J. Geophys. Res.*, **96,** 22 579–22 595.

Schoeberl, M. R., and D. F. Strobel, 1978: The zonally averaged circulation of the middle atmosphere. *J. Atmos. Sci.*, **35,** 577–591.

Smith, W. L., H. M. Woolf, C. M. Hayden, D. Q. Wark, and L. M. McMillin, 1979: The TIROS-N Operational Vertical Sounder. *Bull. Amer. Meteor. Soc.*, **60,** 1177–1187.

Stolarski, R. S., P. Bloomfield, R. D. McPeters, and J. R. Herman, 1991: Total ozone trends deduced from *Nimbus-7* TOMS data. *Geophys. Res. Lett.*, **18,** 1015–1018.

Strobel, D. F., 1978: Parameterization of the atmospheric heating rate from 15 to 120 km due to O_2 and O_3 absorption of solar radiation. *J. Geophys. Res.*, **83,** 6225–6230.

van Loon, H., and K. Labitzke, 1990: Association between the 11-year solar cycle and the atmosphere. Part IV: The stratosphere, not grouped by the phase of the QBO. *J. Climate,* **3,** 827–837.

World Meteorological Organization, 1988: *Report of the International Ozone Trends Panel 1988,* Global Ozone Research and Monitoring Project, Report No. 18, World Meteorological Organization, Geneva, Switzerland, 829 pp.

Wuebbles, D. J., D. E. Kinnison, K. E. Grant, and J. Lean, 1991: The effect of solar flux variations and trace gas emissions on recent trends in stratospheric ozone and temperature. *J. Geomagn. Geoelect.*, **43**(Suppl., Part 2), 709–718.